12

Finite-Difference Time-Domain Methods on Orthogonal Meshes

Up to this point, we have focused on frequency-domain techniques and applications. In this chapter we move to time-domain methods with the goal of simulating the temporal behavior of electromagnetic fields. While integral equation based methods have been employed occasionally in time-domain applications [1, 2], partial differential equation (PDE) based methods have proven to be more practical and have thus seen broader use. Here we discuss in some detail the Cartesian mesh finite-difference time-domain (FDTD) method, the oldest and most widely used of these techniques. This method was first described by K. Yee in 1966 [3]. As computing hardware became faster and more widely available, the method found numerous applications in electromagnetic radiation, scattering, and coupling. Stimulated by these successes, various researchers developed enhancements to the original technique that greatly extended its range of applicability [4–7].

Several key attributes combine to make the FDTD method a useful and powerful tool. First is the method's simplicity; Maxwell's equations in differential form are discretized in space and time in a straightforward manner. Second, since the method tracks the time-varying fields throughout a volume of space, FDTD results lend themselves well to scientific visualization methods. These, in turn, provide the user with excellent physical insights on the behavior of electromagnetic fields. Finally, the geometric flexibility of the method permits the solution of a wide variety of radiation, scattering, and coupling problems.

We will generally limit our discussion in this chapter to the two-dimensional case. This greatly simplifies the exposition of the method while retaining most of its key features. The three-dimensional extension is both notationally and conceptually straightforward. Readers interested in additional information are referred to texts on the subject [8, 9] and to review articles and their extensive bibliographies [10, 11].

12.1 MAXWELL'S EQUATIONS IN THE TIME DOMAIN

The frequency-domain form of Maxwell's equations was presented in Chapter 1. In the time domain, Ampere's and Faraday's laws (the curl equations) take on the forms

$$\frac{\partial \mathbf{D}}{\partial t} = \nabla \times \mathbf{H} - \mathbf{J} \tag{12.1}$$

$$\frac{\partial \mathbf{B}}{\partial t} = -\nabla \times \mathbf{E} \tag{12.2}$$

The divergence equations are unchanged:

$$\nabla \cdot \mathbf{D} = \rho \tag{12.3}$$

$$\nabla \cdot \mathbf{B} = 0 \tag{12.4}$$

In linear, isotropic, time-invariant, nondispersive media, the fluxes (**D** and **B**) and field strengths (**E** and **H**) are related via the material parameters

$$\mathbf{D} = \epsilon \mathbf{E} \tag{12.5}$$

$$\mathbf{B} = \mu \mathbf{H} \tag{12.6}$$

Under these simplifying assumptions, (12.1) and (12.2) can be written as

$$\epsilon \frac{\partial \mathbf{E}}{\partial t} = \nabla \times \mathbf{H} - \mathbf{J} \tag{12.7}$$

$$\mu \frac{\partial \mathbf{H}}{\partial t} = -\nabla \times \mathbf{E} \tag{12.8}$$

These equations form a hyperbolic system of coupled PDEs that are first order in space and time. They can readily be combined to form a single PDE that is second order in both space and time. For example, in the simple case of source-free uniform lossless media, (12.7) and (12.8) can be combined to form

$$\frac{1}{c^2} \frac{\partial^2 \mathbf{E}}{\partial t^2} = \nabla^2 \mathbf{E} \tag{12.9}$$

a second-order wave equation with wave propagation speed $c = 1/\sqrt{\mu\epsilon}$.

12.2 CENTERED FINITE-DIFFERENCE APPROXIMATIONS

Let $f(z)$ be a smooth function. For a sufficiently small interval Δz, df/dz is approximated by a simple two-point finite difference. The highest accuracy occurs when the finite difference is centered as

$$\left.\frac{df}{dz}\right|_{z=z_0} = \frac{f(z_0 + \Delta z/2) - f(z_0 - \Delta z/2)}{\Delta z} + O(\Delta z^2) \tag{12.10}$$

resulting in second-order accuracy. Thus, discretization errors are reduced by a factor of 4 when the mesh size is halved. The FDTD method, like most time-domain PDE methods, is based on the direct solution of (12.7) and (12.8). In the core FDTD algorithm, the continuous derivatives in both space and time are approximated by centered two-point finite differences.

This permits reasonable accuracy at minimal computational expense. The use of higher order methods has been explored [12] but has not yet seen widespread practical use, perhaps due to computational and programming complexity or to the lack of suitable supporting algorithms such as absorbing boundary conditions.

12.3 FDTD SPATIAL DISCRETIZATION

Rather than develop the method in all its detail, consider two-dimensional electromagnetic wave propagation in free space. For TE polarization, Maxwell's curl equations then reduce to

$$\epsilon_0 \frac{\partial E_x}{\partial t} = \frac{\partial H_z}{\partial y} \tag{12.11}$$

$$\epsilon_0 \frac{\partial E_y}{\partial t} = -\frac{\partial H_z}{\partial x} \tag{12.12}$$

$$\mu_0 \frac{\partial H_z}{\partial t} = \frac{\partial E_x}{\partial y} - \frac{\partial E_y}{\partial x} \tag{12.13}$$

The FDTD spatial discretization is developed by positioning the field variables such that all the spatial derivatives can be approximated by two-point, centered differences. The spatial layout is shown in Figure 12.1 with the computational stencil (or molecule) shown in bold. The stencil shows which field variables are computationally connected to which other fields on each time step. The definition of a unit cell within this spatially staggered system is somewhat arbitrary. However, the convention is to define the cells such that the grid lines pass through the electric field variables and coincide with their vector directions. This choice is motivated by the observation that boundary conditions imposed on the electric field are more common in practice than those imposed on the magnetic field. The FDTD programming and mesh generation are thus made somewhat easier.

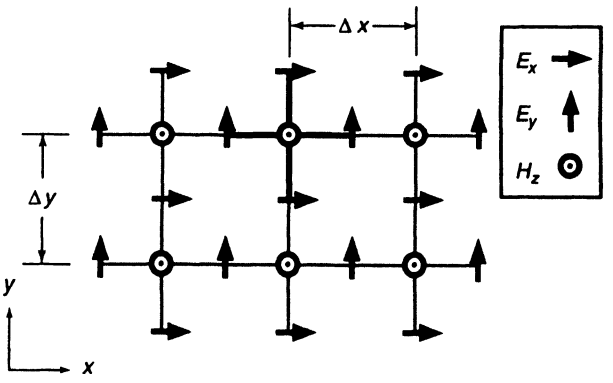

Figure 12.1 Spatial arrangement of field variables in the FDTD method for the two-dimensional TE case.

A word on notation is now in order. A unit cell in the two-dimensional TE case is depicted in Figure 12.2. Let the cell size be $\Delta x \times \Delta y$ and let i and j index the x and y discretizations, respectively. The spatial position of the electric field variables is then

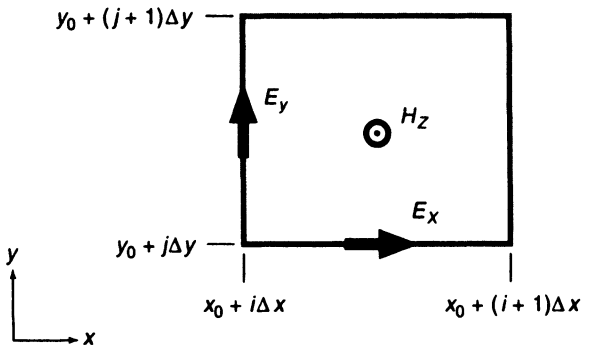

Figure 12.2 The FDTD unit cell for the two-dimensional TE case.

denoted by

$$E_x(i+\tfrac{1}{2}, j) \equiv E_x[x = x_0 + (i+\tfrac{1}{2})\Delta x, y = y_0 + j\Delta y] \tag{12.14}$$

$$E_y(i, j+\tfrac{1}{2}) \equiv E_y[x = x_0 + i\Delta x, y = y_0 + (j+\tfrac{1}{2})\Delta y] \tag{12.15}$$

where (x_0, y_0) is the grid origin. The magnetic field at the cell center is thus $H_z(i+\frac{1}{2}, j+\frac{1}{2})$. This simplified index notation explicitly exposes the half-cell positions of each field variable. Unfortunately, this clear notation cannot be carried over directly into computer software as commonly used programming languages only support arrays with integer indices. Most practitioners adopt the convention of rounding down. For example, the field variable $H_z(i+\frac{1}{2}, j+\frac{1}{2})$ might be associated in code with an array location `HZ(i, j)`. Some authors use this same "rounded-down" notation in publications, thus associating field variables with a particular cell while leaving the precise location within a cell implied. We elect to make the within-cell location explicit.

The FDTD temporal discretization will be discussed in the following section. Superscripts will be used to index time as in

$$E_x^n \equiv E_x(t = t_0 + n\Delta t) \tag{12.16}$$

Using this notation, the spatial FDTD approximation to Equations (12.11)–(12.13) is then

$$\epsilon_0 \dot{E}_x(i+\tfrac{1}{2}, j) = \frac{H_z(i+\frac{1}{2}, j+\frac{1}{2}) - H_z(i+\frac{1}{2}, j-\frac{1}{2})}{\Delta y} \tag{12.17}$$

$$\epsilon_0 \dot{E}_y(i, j+\tfrac{1}{2}) = -\frac{H_z(i+\frac{1}{2}, j+\frac{1}{2}) - H_z(i-\frac{1}{2}, j+\frac{1}{2})}{\Delta x} \tag{12.18}$$

$$\mu_0 \dot{H}_z(i+\tfrac{1}{2}, j+\tfrac{1}{2}) = \frac{E_x(i+\frac{1}{2}, j+1) - E_x(i+\frac{1}{2}, j)}{\Delta y} - \frac{E_y(i+1, j+\frac{1}{2}) - E_y(i, j+\frac{1}{2})}{\Delta x} \tag{12.19}$$

where the dot notation is used to indicate a derivative with respect to time.

The two-dimensional TM case can be derived in a similar fashion. The resultant equations are essentially the dual of (12.17)–(12.19). However, our convention that the discrete electric field variables live on and parallel to the cell edges dictates a half-cell shift in both x and y as shown in Figure 12.3.

An alternate derivation of the FDTD method can be obtained by approximating the integral form of Maxwell's curl equations (Ampere's and Faraday's laws):

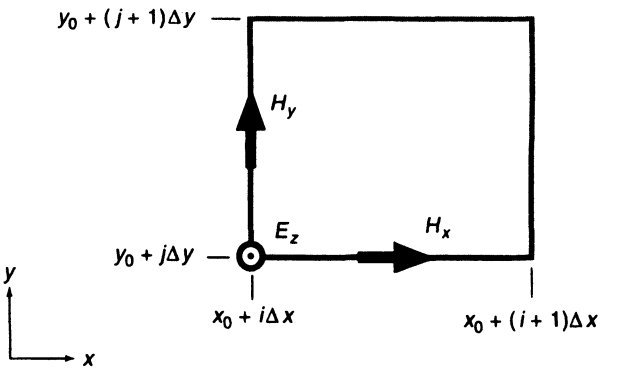

Figure 12.3 The FDTD unit cell for the two-dimensional TM case.

$$\iint_A \dot{\mathbf{D}} \cdot \hat{n}\, dA = \oint_{\partial A} \mathbf{H} \cdot \mathbf{dl} \tag{12.20}$$

$$\iint_A \dot{\mathbf{B}} \cdot \hat{n}\, dA = -\oint_{\partial A} \mathbf{E} \cdot \mathbf{dl} \tag{12.21}$$

where A is some area, ∂A denotes the boundary of that area, and $\hat{n}$ is a unit vector normal to A. Local spatial approximations to these equations form the theoretical basis for a family of related techniques known as finite-volume, finite-integration, or control region methods. These types of formulations have proven useful in developing extensions and generalizations of the basic FDTD method, for example, thin-wire approximations and nonorthogonal grid techniques.

As an example of this integral approach, refer to Figure 12.2 and consider approximating Faraday's law over an FDTD unit cell. Assume that the magnetic field is constant over the cell and that the electric fields are constant along each edge. Then, Faraday's law becomes

$$\begin{aligned} \mu_0 \dot{H}_z(i+\tfrac{1}{2}, j+\tfrac{1}{2})\, \Delta x\, \Delta y &\approx -\sum_{\text{sides}} E_{\text{side}}\, \text{length}_{\text{side}} \\ &= -E_x(i+\tfrac{1}{2}, j)\, \Delta x + E_y(i, j+\tfrac{1}{2})\, \Delta y \\ &\quad + E_x(i+\tfrac{1}{2}, j+1)\, \Delta x - E_y(i+1, j+\tfrac{1}{2})\, \Delta y \end{aligned} \tag{12.22}$$

By dividing the left- and right-hand sides of this equation by $\Delta x\, \Delta y$, this result is shown to be identical to the differential formulation. A similar procedure can also be used for discretizing Ampere's law.

12.4 FDTD TIME DISCRETIZATION

The same centered-difference concepts are used to advance the fields in time. This requires that **E** and **H** be staggered in time by one half of a time step. Let **E** be defined at integer time steps with **H** at the half-integer time points. The temporal discretization is then

$$\epsilon_0 \dot{\mathbf{E}}^{n-1/2} \approx \epsilon_0 \frac{\mathbf{E}^n - \mathbf{E}^{n-1}}{\Delta t} = \nabla \times \mathbf{H}^{n-1/2} \tag{12.23}$$

$$\mu_0 \dot{\mathbf{H}}^n \approx \mu_0 \frac{\mathbf{H}^{n+1/2} - \mathbf{H}^{n-1/2}}{\Delta t} = -\nabla \times \mathbf{E}^n \tag{12.24}$$

The spatial discretization is as in the previous section. These expressions can be rearranged to generate a time advancement procedure

$$\mathbf{E}^n = \mathbf{E}^{n-1} + \frac{\Delta t}{\epsilon_0} \nabla \times \mathbf{H}^{n-1/2} \tag{12.25}$$

$$\mathbf{H}^{n+1/2} = \mathbf{H}^{n-1/2} - \frac{\Delta t}{\mu_0} \nabla \times \mathbf{E}^n \tag{12.26}$$

This method, known as leap-frog time integration, is depicted graphically in Figure 12.4. Fields are advanced in time by using information from the opposite field type at an intermediate time point. Note that the method is explicit; calculations depend only on results at earlier times, again contributing to the computational efficiency of the FDTD method.

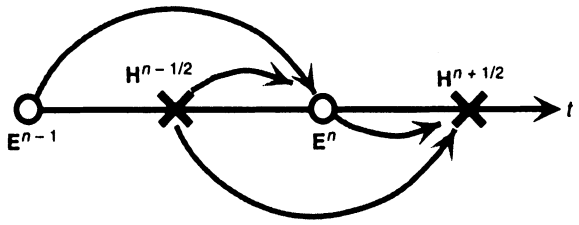

Figure 12.4 Leap frog time integration.

12.5 DIVERGENCE CONSERVATION IN THE FDTD

Up to this point we have worked with Maxwell's curl equations (12.1) and (12.2) while ignoring the divergence equations (12.3) and (12.4). The reasons for this are clear in the continuous analytic case, as divergence conditions are not independent and can be derived from the curl equations. To verify that this remains true under FDTD discretization, we investigate a discrete version of Gauss' law. In free space, Gauss' law states

$$\nabla \cdot \mathbf{D} = 0 \Longrightarrow \oint_{\partial A} \mathbf{D} \cdot \hat{n}\, dl = 0 \tag{12.27}$$

where ∂A is the boundary of some region A with unit normal $\hat{n}$. In the TE polarization, the staggered FDTD mesh lends itself to a discretized version of (12.27) evaluated over the region depicted in Figure 12.5. This region is shifted a half cell from the usual FDTD grid so that electric field unknowns are perpendicular to the region. To simplify the analysis, we have reindexed the cells locally. Equation (12.27) then becomes

$$\oint_{\partial A} \mathbf{D} \cdot \hat{n}\, dl \approx D_x^+ \, \Delta y + D_y^+ \, \Delta x - D_x^- \, \Delta y - D_y^- \, \Delta x \tag{12.28}$$

Differentiating (12.28) with respect to time and using (12.17) and (12.18) yields

$$\left(\frac{H_1 - H_4}{\Delta y}\right) \Delta y + \left(\frac{H_2 - H_1}{\Delta x}\right) \Delta x - \left(\frac{H_2 - H_3}{\Delta y}\right) \Delta y - \left(\frac{H_3 - H_4}{\Delta x}\right) \Delta x = 0 \tag{12.29}$$

This discrete measure of divergence is conserved locally by the FDTD algorithm. Thus, if the initial conditions are divergence free, then Gauss' law is satisfied throughout an FDTD calculation.

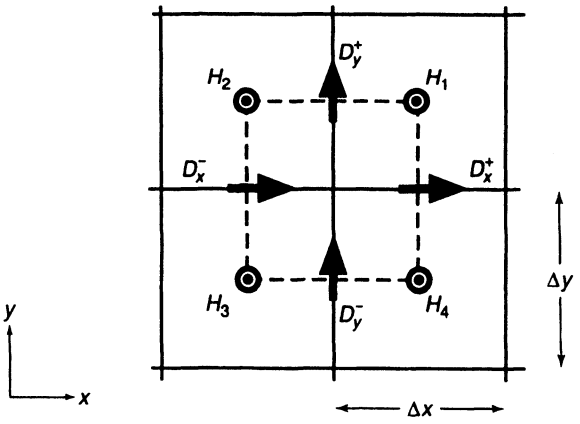

Figure 12.5 Integration region and field variables for an FDTD implementation of Gauss' law.

12.6 EXTENSION TO THREE DIMENSIONS

The three-dimensional case can be derived readily using the same techniques (differential or integral) used previously for the two-dimensional case. Alternatively, one can infer the three-dimensional case by "gluing" together two-dimensional cells from each of the three orthogonal planes, $x-y$, $y-z$, and $z-x$. A full three-dimensional FDTD cell (Yee lattice) is shown in Figure 12.6. As in the two-dimensional case, the custom in programming is to round down half-integer indices. The leap frog integration method is used to advance the time step.

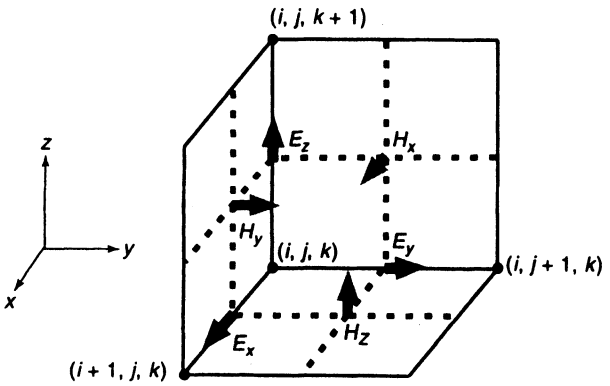

Figure 12.6 Three-dimensional staggered mesh FDTD cell (Yee lattice).

12.7 OTHER COORDINATE SYSTEMS

The FDTD method can also be used in other orthogonal coordinate systems. For instance, consider the two-dimensional TE case in polar coordinates. Maxwell's curl equations in free space are then

$$\epsilon_0 \dot{E}_r = \frac{1}{r}\frac{\partial H_z}{\partial \phi} \tag{12.30}$$

$$\epsilon_0 \dot{E}_\phi = -\frac{\partial H_z}{\partial r} \tag{12.31}$$

$$\mu_0 \dot{H}_z = \frac{1}{r}\frac{\partial E_r}{\partial \phi} - \frac{1}{r}\frac{\partial (r E_\phi)}{\partial r} \tag{12.32}$$

The spatial stencil/FDTD unit cell shown in Figure 12.7 permits centered spatial differencing. Some care is required to handle the $1/r$ factors. For instance, the spatial discretization of (12.32) is

$$\begin{aligned}\mu_0 \dot{H}_z(i+\tfrac{1}{2}, j+\tfrac{1}{2}) = {} & \frac{E_r(i+\tfrac{1}{2}, j+1) - E_r(i+\tfrac{1}{2}, j)}{r_{i+1/2}\,\Delta\phi} \\ & - \frac{r_{i+1}E_\phi(i+1, j+\tfrac{1}{2}) - r_i E_\phi(i, j+\tfrac{1}{2})}{r_{i+1/2}\,\Delta r}\end{aligned} \tag{12.33}$$

where $r_i = i\,\Delta r$, $r_{i+1/2} = (i+\frac{1}{2})\,\Delta r$, and so on.

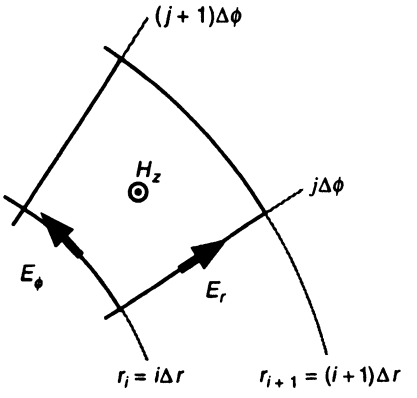

Figure 12.7 Two-dimensional FDTD cell in polar coordinates.

12.8 NUMERICAL ANALYSIS OF THE FDTD ALGORITHM: STABILITY, DISPERSION, AND ANISOTROPY

In this section we investigate the accuracy and stability of the FDTD algorithm. That is, how well do solutions to the finite-difference approximations introduced in the previous sections approximate the true behavior of the continuous PDEs? And, what conditions are required for an FDTD calculation to remain bounded?

For simplicity, consider the case of one-dimensional propagation in the x direction. Maxwell's curl equations can be combined to form a one-dimensional, second-order wave equation

$$\frac{1}{c^2}\frac{\partial^2 E}{\partial t^2} = \frac{\partial^2 E}{\partial x^2} \tag{12.34}$$

It is straightforward to show that the FDTD discretization (staggered spatial mesh with leap frog time integration) of the first-order Maxwell equations is numerically equivalent to discretizing (12.34) with the standard three-point centered finite-difference approximation to the second derivative

$$\frac{E^{n+1}(i) - 2E^n(i) + E^{n-1}(i)}{(c\,\Delta t)^2} = \frac{E^n(i+1) - 2E^n(i) + E^n(i-1)}{\Delta x^2} \tag{12.35}$$

This second-order difference equation is sometimes easier to work with as the half-integer quantities (space and time indices on H) are eliminated.

Stability analysis starts by looking for solutions of Equation (12.35) that are wave like in space,

$$E^n(i) = \xi^n e^{-jkx}\big|_{x=i\,\Delta x} \tag{12.36}$$

where $j = \sqrt{-1}$ and $k = 2\pi/\lambda$ is the wavenumber. The solution will then be growing, shrinking, or oscillating in time depending on the magnitude of ξ. Plugging this expression into the second-order difference equation and eliminating the common factors give

$$\xi^2 - 2A\xi + 1 = 0 \tag{12.37}$$

where

$$A = 1 - 2\left(\frac{c\,\Delta t}{\Delta x}\right)^2 \sin^2\left(\frac{k\,\Delta x}{2}\right) \tag{12.38}$$

hence

$$\xi = A \pm (A^2 - 1)^{1/2} \tag{12.39}$$

A growing (unstable) solution will occur if $|\xi| > 1$. This can only occur if $|A| > 1$. Thus,

$$c\,\Delta t > \Delta x \Longrightarrow \text{instability} \tag{12.40}$$

Alternatively, if $|A| \leq 1$, then $c\,\Delta t \leq \Delta x$ and

$$|\xi| = \left|A + j(1 - A^2)^{1/2}\right| = 1 \tag{12.41}$$

implying an oscillating (wavelike) solution in time.

In a one-dimensional FDTD code, $c\,\Delta t \leq \Delta x$ is required for stability. This constraint is known as the Courant stability condition and is easy to interpret physically. When the Courant stability condition is satisfied, the FDTD grid is causally connected; the speed of light bounds the rate at which information can be transmitted across the mesh.

In higher dimensions, say three, the stability criterion becomes

$$c\,\Delta t \leq \frac{1}{\left(1/\Delta x^2 + 1/\Delta y^2 + 1/\Delta z^2\right)^{1/2}} \tag{12.42}$$

Thus, for the cubical grid case ($\Delta x = \Delta y = \Delta z$), Δt must be chosen such that $c\,\Delta t \leq \Delta x/\sqrt{3} \approx 0.577\,\Delta x$. Similarly, in the two-dimensional square mesh case, stable solutions require that $c\,\Delta t \leq \Delta x/\sqrt{2} \approx 0.707\,\Delta x$. The reason for smaller stability limits in higher dimensions can be in Figure 12.8. Here, a plane wave is propagating on a two-dimensional square-cell FDTD mesh along the mesh diagonals. Projecting lines of constant phase onto an equivalent one-dimensional mesh results in an effective mesh spacing of $\Delta x/\sqrt{2}$. The time step must be reduced in size accordingly to ensure stability on this smaller effective mesh.

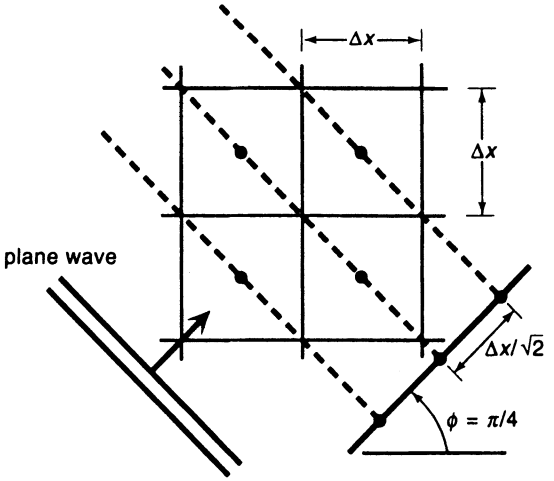

Figure 12.8 Plane-wave propagation along the diagonal of a two-dimensional square-cell ($\Delta x \times \Delta x$) mesh is equivalent to one-dimensional propagation along a mesh with cell size $\Delta x/\sqrt{2}$, thus accounting for the two-dimensional stability limit of $c\,\Delta t \leq \Delta x/\sqrt{2}$.

The stability analysis presented here applies to the uniform media (constant c) case. When a simulation geometry contains several materials with differing values of c, this same Courant condition can be applied, provided the maximum value of c is used.

Satisfaction of the Courant stability limit only ensures that the numerical solution remains bounded. The accuracy of the numerical solution is the next topic to address. In free space all plane waves propagate at the same speed, independent of frequency or wavenumber. This is not the case on an FDTD grid. This phenomenon is known as numerical dispersion, and its analysis is similar to the stability analysis on the previous few pages. First consider the one-dimensional, uniform media case. Assume wavelike solutions:

$$E^n(i) = e^{j(\omega n\,\Delta t - ki\,\Delta x)} \tag{12.43}$$

where ω is the temporal frequency of the wave in radians/sec. We then seek information about the relationship between ω and the wavenumber k.

Substituting (12.43) into the discretized one-dimensional wave equation (12.35) and doing some algebra yields the dispersion relation for the FDTD method:

$$\frac{1}{(c\,\Delta t)^2}\sin^2\left(\frac{\omega}{c}\frac{c\,\Delta t}{2}\right) = \frac{1}{\Delta x^2}\sin^2\left(\frac{k\,\Delta x}{2}\right) \tag{12.44}$$

In the limit, as $\omega\,\Delta t$ and $k\,\Delta x$ go to zero, this equation recovers the dispersion relation for the continuous case:

$$\left(\frac{\omega}{c}\right)^2 = k^2 \tag{12.45}$$

Here the phase velocity $v_p \equiv \omega/k$ is a constant. The FDTD dispersion relation also recovers the exact solution when $c\,\Delta t = \Delta x$ (right at the Courant limit). This is rarely a practical result as it only occurs in the one-dimensional, homogeneous media case.

For finite Δt and Δx, the numerical dispersion relation differs from the ideal, continuous solution case. Define an ideal solution wavelength as $\lambda_0 \equiv cT$, where $T = 2\pi/\omega$ is the temporal period. In the discrete case, the spatial wavelength realized on the grid is $\lambda_g = 2\pi/k$. The phase velocity and the grid wavelength are two measures of numerical

dispersion and are related by

$$\frac{v_p}{c} = \frac{\lambda_g}{\lambda_0} \tag{12.46}$$

Define a Courant or stabilty ratio as $\alpha = c\ \Delta t/\Delta x$. Solutions of the dispersion relation (12.44) in terms of these new variables are shown in Figure 12.9. The normalized phase velocity v_p/c is plotted as a function of the normalized cell size for various values of the Courant ratio. The FDTD phase velocity errors are small for well-resolved waves but increase rapidly as the cell size increases. The use of small relative time steps (small Courant ratios) also increases dispersion errors.

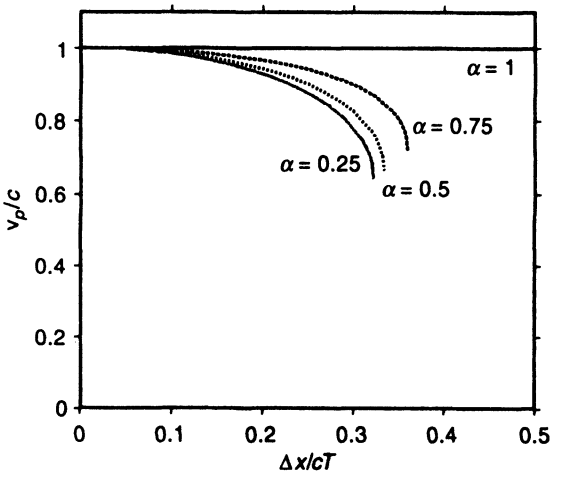

Figure 12.9 Numerical dispersion in the one-dimensional method: the normalized phase velocity v_p/c is plotted as a function of the normalized cell size for various values of the Courant stability ratio α.

A time-limited signal or pulse contains a spectrum of frequencies. As different frequencies propagate at different speeds on the FDTD grid, the impact of numerical dispersion is to distort pulses as they propagate through the mesh. As an example, the left-hand boundary of a one-dimensional FDTD grid is driven with a signal

$$f(t) = \begin{cases} 0.5\left[1 - \cos\left(\dfrac{2\pi t}{T}\right)\right] & 0 \le t \le T \\ 0 & \text{otherwise} \end{cases} \tag{12.47}$$

This pulse has an initial spatial width of cT, and it propagates through the FDTD grid from left to right. Cell size was chosen to resolve the pulse fairly well, $\Delta x/cT = \frac{1}{10}$. The Courant ratio was set to the value commonly used in higher dimensional applications, $c\ \Delta t/\Delta x = \frac{1}{2}$. In Figure 12.10, the initial pulse shape is shown along with its result after propagating down the mesh for four pulse widths. Note the change in pulse shape and the trailing-edge distortion. These effects can, of course, be reduced by using a finer mesh.

In two dimensions, the numerical dispersion relation is

$$\frac{1}{(c\ \Delta t)^2}\sin^2\left(\frac{\omega}{c}\frac{c\ \Delta t}{2}\right) = \frac{1}{\Delta x^2}\sin^2\left(\frac{k_x\ \Delta x}{2}\right) + \frac{1}{\Delta y^2}\sin^2\left(\frac{k_y\ \Delta y}{2}\right) \tag{12.48}$$

where k_x and k_y are the wavenumbers in the x and y directions, respectively. In addition to numerical dispersion effects as observed in one dimension, phase velocity in higher dimensions is a function of the angle of propagation through the mesh. This effect is known as grid anisotropy. In Figure 12.11, the normalized phase velocity is plotted as a function

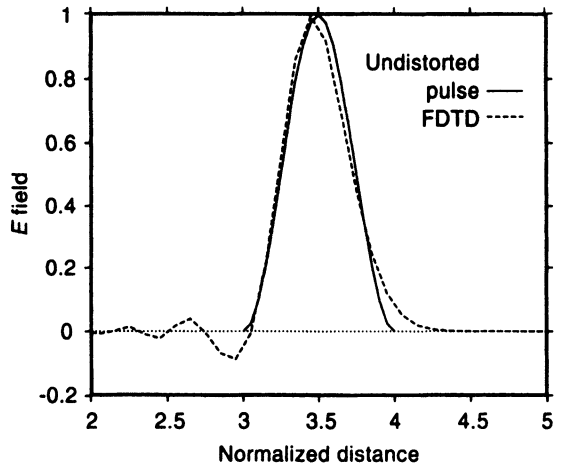

Figure 12.10 Pulse distortion due to numerical dispersion.

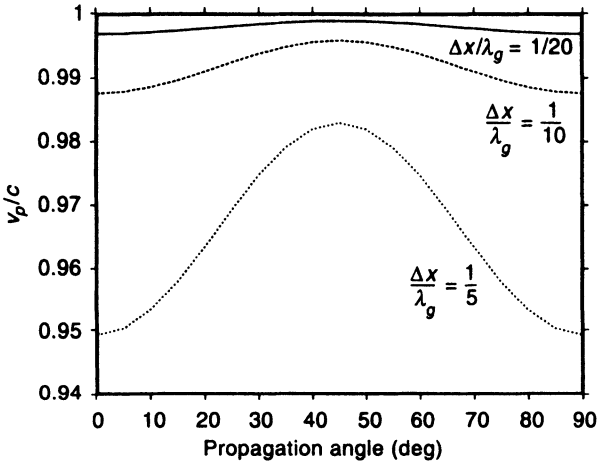

Figure 12.11 Grid anisotropy in the two-dimensional FDTD method. Normalized phase velocity v_p/c is plotted as a function of propagation angle for various cell sizes. Cells are square and $c\,\Delta t/\Delta x = \frac{1}{2}$; 0° and 90° angles correspond to propagation along the grid lines.

of wave angle for various values of the stability ratio. Errors due to grid anisotropy are generally smaller than those due to simple numerical dispersion.

12.9 TREATING LOSSY/CONDUCTIVE MEDIA

Up to this point we have focused on the use of the FDTD algorithm in uniform lossless material. To use this method to solve practical problems, we need to develop mechanisms for handling various boundary conditions, sources, and realistic materials. We first examine a simple modification to the FDTD algorithm that permits the use of lossy, conductive material. A side effect of this algorithm modification is a simple and efficient way to handle p.e.c. boundary conditions.

In materials with finite conductivity, an ohmic loss current is induced with $\mathbf{J} = \sigma\mathbf{E}$. Substituting this into Ampere's law and discretizing in time,

$$\epsilon\dot{\mathbf{E}}^{n-1/2} = \nabla \times \mathbf{H}^{n-1/2} - \sigma\mathbf{E}^{n-1/2} \tag{12.49}$$

Since $\mathbf{E}$ is only known at integer times, the conductive loss term needs to be implemented using a time average

$$\epsilon \frac{\mathbf{E}^n - \mathbf{E}^{n-1}}{\Delta t} = \nabla \times \mathbf{H}^{n-1/2} - \sigma \frac{\mathbf{E}^n + \mathbf{E}^{n-1}}{2} \tag{12.50}$$

Fortunately, $\mathbf{E}^n$ can be isolated algebraically and an implicit calculation avoided:

$$\mathbf{E}^n = \frac{1 - \sigma\ \Delta t/2\epsilon}{1 + \sigma\ \Delta t/2\epsilon} \mathbf{E}^{n-1} + \frac{1}{1 + \sigma\ \Delta t/2\epsilon} \frac{\Delta t}{\epsilon} \nabla \times \mathbf{H}^{n-\frac{1}{2}} \tag{12.51}$$

In addition to handling lossy material, this expression presents us with one way of handling a p.e.c. boundary condition. When $\sigma >> 1$, (12.51) reduces to $\mathbf{E}^n \approx -\mathbf{E}^{n-1}$. Thus, if the components of $\mathbf{E}$ tangential to a p.e.c. boundary are initialized to zero, they will remain nearly zero throughout the calculation. This method for imposing p.e.c. boundary conditions is particularly efficient in general-purpose FDTD codes as it directly employs the ordinary FDTD equations without the need for additional tests or loops.

12.10 FREQUENCY-DEPENDENT MEDIA

The FDTD equations developed in Sections 12.3 and 12.4 are based on the presumption that the instantaneous fluxes and field strengths are linearly related through constant material parameters ϵ and μ. This simple relationship is exact in free-space calculations, and it suffices as a description of many materials over a narrow to moderate frequency range. However, more involved flux–field relationships are required for modeling some common materials (e.g., water), especially when wide-band results are desired. The original FDTD field update equations will need to be modified to accommodate these materials.

Material parameters are typically reported by experimentalists and vendors as functions of frequency; the linear relationship between fields and fluxes holds at each frequency

$$\tilde{\mathbf{D}}(\omega) = \epsilon_r^*(\omega)\epsilon_0 \tilde{\mathbf{E}}(\omega) \tag{12.52}$$

where $\epsilon_r^*(\omega)$ is a complex relative dielectric function that may or may not incorporate the bulk conductivity. The time-domain equivalent of (12.52) is the convolution integral:

$$\mathbf{D}(t) = \epsilon_0 \int_0^t \mathbf{E}(t - \tau)\epsilon_r(\tau)\, d\tau \tag{12.53}$$

There are two significant practical problems with a naive direct FDTD implementation of (12.53). First, the convolution integral needs to be reevaluated every time step for each electric field variable within the frequency-dependent media. Second, and more importantly, calculation of the convolution requires storage of the electric field time histories. While we should expect some increase in operation count and memory requirements to be able to handle these materials, the costs articulated here would overwhelm most computational resources when used in three-dimensional simulations with dispersive materials of significant spatial extent.

Luebbers et al. [13] developed a computationally efficient way of implementing (12.53) within the FDTD context by first recognizing that Ampere's law actually deals with $\partial \mathbf{D}/\partial t$ and not $\mathbf{D}$ directly and then by choosing representations of $\epsilon_r(t) \leftrightarrow \epsilon_r^*(\omega)$ that are analytically suitable. In [8], FDTD modifications for handling several different

classes of frequency-dependent materials are discussed. We limit our discussion here to the simplest of these, Debye materials.

Debye materials are characterized by a frequency-domain permittivity with a single complex pole

$$\epsilon_r^*(\omega) = \epsilon_\infty + \frac{\epsilon_s - \epsilon_\infty}{1 + j\omega t_0} \tag{12.54}$$

where ϵ_∞ is the relative permittivity at high frequency, ϵ_s is the relative permittivity in the static limit, and t_0 is a characteristic relaxation time for the material. Let the second term on the right-hand side of (12.54) be $\chi(\omega)$, a frequency-dependent electric susceptibility.[1] In the time domain,

$$\chi(t) = \frac{\epsilon_s - \epsilon_\infty}{t_0} e^{-t/t_0} U(t) \tag{12.55}$$

where $U(t)$ is the unit step function.

Discretizing (12.53) results in

$$\mathbf{D}^n = \epsilon_0 \left(\epsilon_\infty \mathbf{E}^n + \sum_{m=0}^{n-1} \mathbf{E}^{n-m} \int_{m\Delta t}^{(m+1)\,Dt} \chi(\tau)\, d\tau \right) \tag{12.56}$$

Developing an analogous expression for $\mathbf{D}^{n-1}$ and defining

$$\bar{\chi}^0 \equiv \int_0^{\Delta t} \chi(\tau)\, d\tau \tag{12.57}$$

and

$$\Delta\chi^m \equiv \int_{m\,\Delta t}^{(m+1)\,\Delta t} \chi(\tau)\, d\tau - \int_{(m+1)\,\Delta t}^{(m+2)\,\Delta t} \chi(\tau)\, d\tau \tag{12.58}$$

lead to the modified FDTD electric field temporal update equation

$$\mathbf{E}^n = \frac{\epsilon_\infty}{\epsilon_\infty + \bar{\chi}^0} \left(\mathbf{E}^{n-1} + \frac{1}{\epsilon_\infty} \Psi^{n-1} + \frac{\Delta t}{\epsilon_\infty \epsilon_0} \nabla \times \mathbf{H}^{n-1/2} \right) \tag{12.59}$$

where we have introduced a new variable Ψ to absorb the convolution summation

$$\Psi^{n-1} = \sum_{m=0}^{n-2} \mathbf{E}^{n-1-m}\, \Delta\chi^m \tag{12.60}$$

Evaluation of (12.60) still appears to require saving the electric field time histories. Fortunately, the exponential form of $\chi(t)$ allows us to greatly simplify this calculation. Evaluating (12.58) yields

$$\Delta\chi^m = (\epsilon_s - \epsilon_\infty)(1 - e^{-\Delta t/t_0})^2 e^{-m\,\Delta t/t_0} \tag{12.61}$$

from which we note that

$$\Delta\chi^{m+1} = e^{-\Delta t/t_0}\, \Delta\chi^m \tag{12.62}$$

and

$$\Psi^{n-1} = \mathbf{E}^{n-1}\, \Delta\chi^0 + e^{-\Delta t/t_0} \Psi^{n-2} \tag{12.63}$$

[1] Note that this is a different definition of susceptibility than is found in most introductory electromagnetics textbooks where $\epsilon_r \equiv 1 + \chi$.

The convolution sum is thus reduced to a running sum, eliminating the need to store electric field time histories. Frequency-dependent materials amenable to the Debye model can thus be handled efficiently. When compared with the standard, simple media FDTD equations, the modified equations presented here require several more operations and the addition of an additional auxiliary field variable, Ψ. These costs seem reasonable given the added modeling capability.

Similar modified FDTD schemes have been developed for several other (non-Debye) classes of materials. The basic approach follows that presented here, combining a judicious choice of the analytic form of $\epsilon_r^*(\omega)$ with the use of auxiliary variables to eliminate the time-domain convolution. An alternate ordinary differential equation based approach was developed by Joseph et al. [14]. Following the general linear media constitutive relation given in Harrington [15],

$$\mathbf{D} = \epsilon \mathbf{E} + \epsilon_1 \frac{\partial \mathbf{E}}{\partial t} + \epsilon_2 \frac{\partial^2 \mathbf{E}}{\partial t^2} + \cdots \tag{12.64}$$

Or, even more generally, replace the left-hand side of (12.64) with an expansion in $\mathbf{D}$ and its derivatives with respect to time. In the frequency domain, the resultant complex dielectric constant is expressed as a simple ratio of polynomials with coefficients and order that can be fit to a wide range of materials. Equation (12.64) (or its generalization) is then approximated using finite differences and used to develop modified FDTD update equations. This technique requires that the flux $\mathbf{D}$ be updated and stored, thus incurring a significant but reasonable computational cost.

12.11 SIMPLE BOUNDARY AND INTERFACE CONDITIONS

Next we address the FDTD implementation of simple boundary conditions such as perfect electric conductors, perfect magnetic conductors (p.m.c.), and dielectric material interfaces. In Section 12.9 we used the ordinary FDTD update equations and high values of σ to indirectly but efficiently implement a perfect electric conductor. An alternate and perhaps more direct method is to construct the FDTD grid such that the p.e.c. boundaries coincide with the edges of the unit cells and thus with the appropriate tangential components of the electric field. In a total-field formulation of the FDTD (see Section 12.13 for further discussion of total- vs. scattered-field FDTD formulations), the p.e.c. boundary condition is imposed by setting $E_{\tan} = 0$. This can be accomplished either by maintaining the initial conditions throughout a calculation or by resetting the appropriate electric field components to zero on each time step. In a scattered-field formulation of the FDTD, p.e.c. boundaries must be driven with the negative of the instantaneous incident electric field.

It is sometimes useful to set $H_{\tan} = 0$, for instance to model a p.m.c. or, more likely, to invoke a particular symmetry condition. By analogy with the p.e.c. boundary, this is readily accomplished by passing the perfect magnetic conducting boundary through the center of the cells and thus through the tangential magnetic fields. While simple and direct, this approach has the disadvantage that the mesh generation system must be able to deal with boundaries at both unit and half-cell locations. It is thus desirable to develop a method for positioning a p.m.c. at an FDTD cell edge. Consider the FDTD cells and perfect magnetic

conducting boundary shown in Figure 12.12. The ordinary FDTD field advance for E_x is

$$\epsilon_0 \dot{E}_x(\text{on grid line}) = \frac{H_z(\text{above}) - H_z(\text{below})}{\Delta y} \tag{12.65}$$

A perfect magnetic conducting boundary is equivalent to an antisymmetry condition on H_z, that is, $H_z(\text{below}) = -H_z(\text{above})$. Hence, at a p.m.c.

$$\epsilon_0 \dot{E}_x(\text{at boundary}) = \frac{2H_z(\text{above})}{\Delta y} \tag{12.66}$$

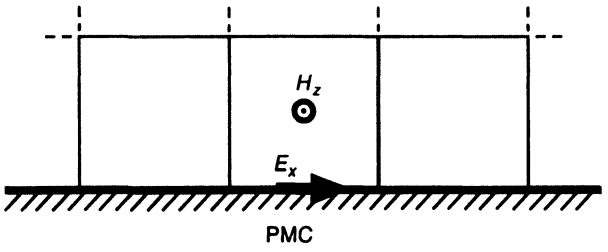

Figure 12.12 Field locations for the PMC boundary condition implementation given by Equation (12.66).

Material parameters such as ϵ, μ, and σ can be set for each field component in each cell. Material interface conditions are generally imposed by simply setting these parameters appropriately. The spatially staggered FDTD mesh makes it difficult to change both the electric and magnetic properties of a material at exactly the same location while simultaneously maintaining continuity of tangential fields and normal fluxes, although this is rarely a significant practical concern.

12.12 ABSORBING BOUNDARY CONDITIONS

To use the FDTD method to solve open-region problems, we require some mechanism for truncating the mesh at a finite distance from the computational region of interest. Ideally, this mechanism [known alternately as an absorbing or radiation boundary condition (ABC or RBC)] should permit electromagnetic energy to pass out of the problem space without distorting the fields or reflecting energy back into computational domain. If possible, the ABC should be computationally efficient, not adding substantial overhead to the core FDTD calculation.

The development of suitable ABCs has been an active area of research for the last two decades. A variety of approaches have been employed, including:

- *Field extrapolation.* In this approach, the fields are extrapolated one cell out from the FDTD computational grid using a cylindrical (two-dimensional) or spherical (three-dimensional) extrapolation or by using Huygens' principle. The extrapolated fields are then used in the ordinary FDTD formulas to update the fields on the boundary. This approach has been reasonably successful, although it forces the user to pick an origin for the expansion. The method may then fail for objects with multiple scattering centers.

- *Impedance conditions.* Electric and magnetic fields perpendicular to the boundary are assumed to be normally propagating plane waves, thus related by the wave impedance. While simple and intuitive, this method only works well when the outgoing waves actually impinge on the boundary at near-normal angles.
- *Surface integrals.* Equivalence principles are used to create virtual surface currents over the exterior of the computational grid; rigorous surface integral formulations are used to extrapolate the fields. While this method can be highly effective, the global nature of the calculations makes the method computationally intractable for most problems.
- *Absorbing material.* This technique wraps the core computational domain with a layer of absorbing material, creating a numerical anechoic chamber. Early versions of this technique were reasonably successful but computationally expensive as thick absorbing layers were required. Recent developments [16] appear to have overcome this difficulty and will be discussed below.
- *One-way wave equations.* This approach has proven to be a productive area for the development of practical and effective ABCs. We will discuss this approach in detail here.

The one-way wave equation approach to the development of ABCs has been employed by many researchers. Seminal works include those by Lindman [17], Engquist and Majda [18], and Mur [19]. Alternative and/or higher order methods are described in [20, 21]. We will focus on the commonly used low-order schemes developed by Mur.

To clarify the discussion, let u represent any generic field component and write the second-order wave equation as

$$\frac{1}{c^2}\partial_t^2 u = \partial_x^2 u + \partial_y^2 u \tag{12.67}$$

where the operator notation ∂_t^2 is used to compactly represent $\partial^2/\partial t^2$. Equation (12.67) supports omnidirectional wave propagation with a dispersion relation

$$\left(\frac{\omega}{c}\right)^2 = k_x^2 + k_y^2 \tag{12.68}$$

The basic concept of a one-way wave equation is a separate PDE that supports wave propagation in some directions but not in others. Ideally, its dispersion relation approximates (12.68) for the desired outgoing directions. Figure 12.13 illustrates the use of this PDE as an ABC. Here, we consider the computational space to be the $+x$ half plane. The standard FDTD equations are used throughout the region $x > 0$. A discrete approximation to a one-way wave equation that supports $-x$ propagating waves only is used as the boundary condition at $x = 0$.

To develop one-way wave equations, we first drop to one-dimension where the second-order wave equation

$$\partial_x^2 u - \frac{1}{c^2}\partial_t^2 u = 0 \tag{12.69}$$

supports bidirectional wave propagation, $u = u(x \pm ct)$. The wave equation can be factored by treating the differential operators ∂_t and ∂_x algebraically:

$$(\partial_x - \frac{1}{c}\partial_t)(\partial_x + \frac{1}{c}\partial_t)u = 0 \tag{12.70}$$

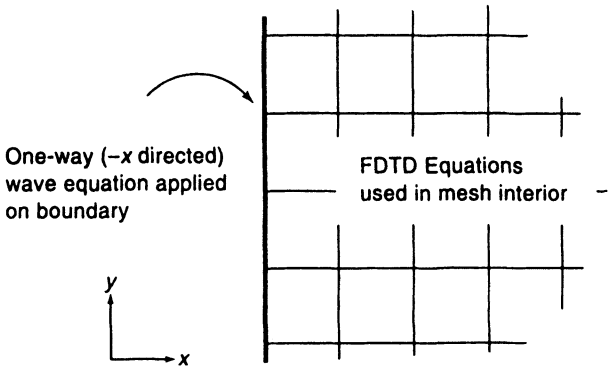

Figure 12.13 One-way wave equation used as an absorbing boundary condition.

Applying each factor to u individually and equating the two results to zero give the one-way wave equations

$$(\partial_x - \frac{1}{c}\partial_t)u = 0 \tag{12.71}$$

$$(\partial_x + \frac{1}{c}\partial_t)u = 0 \tag{12.72}$$

Solutions to (12.71) are $-x$ traveling waves, $u(x + ct)$, while solutions to (12.72) are $+x$ propagating waves of the form $u(x - ct)$. Thus, to simulate an open-region problem, Equations (12.71) and (12.72) are used as boundary conditions on the left and right boundaries, respectively. The use of these one-way wave equations as ABCs is equivalent to the use of an impedance condition.

While the simple impedance condition developed above is occasionally used in higher dimensional computations, it is beneficial to seek one-way wave equations that can better handle nonnormally incident waves. In two dimensions, the second-order wave equation

$$\partial_x^2 u + \partial_y^2 u - \frac{1}{c^2}\partial_t^2 u = 0 \tag{12.73}$$

supports omnidirectional wave propagation. To develop one-way wave equations that are suitable for use as ABCs on the left ($-x$-directed waves) or right ($+x$-directed waves) edges of a computational region, first factor the wave equation as before:

$$\left(\partial_x - \sqrt{\frac{1}{c^2}\partial_t^2 - \partial_y^2}\right)\left(\partial_x + \sqrt{\frac{1}{c^2}\partial_t^2 - \partial_y^2}\right)u = 0 \tag{12.74}$$

Applying each of the factors to u individually gives a one-way wave equation. For instance, on the left wall,

$$\left(\partial_x - \sqrt{\frac{1}{c^2}\partial_t^2 - \partial_y^2}\right)u = 0 \tag{12.75}$$

is the appropriate ABC.

We are then challenged with the interpretation and computation of (12.75). The cavalier algebraic use of partial-derivative operators has led to a pseudo-differential operator that mixes a square-root function with the partial-derivative operators. It is perhaps obvious

but worth emphasizing that

$$\left(\sqrt{\frac{1}{c^2}\partial_t^2 - \partial_y^2}\right) u \neq \sqrt{\frac{1}{c^2}\partial_t^2 u - \partial_y^2 u}\,! \tag{12.76}$$

To interpret this pseudo-differential operator and work toward a computable approximation, consider Fourier transforming u in y and t, with $y \to k_y$ and $t \to \omega$. Thus,

$$u(x, y, t) = F^{-1}\{\tilde{u}(x, k_y, \omega)\} \tag{12.77}$$

and

$$\partial_t u = F^{-1}\{j\omega\tilde{u}\} \qquad \partial_y u = F^{-1}\{jk_y\tilde{u}\} \tag{12.78}$$

The questionable square-root operator is then *defined* by

$$\left(\sqrt{\frac{1}{c^2}\partial_t^2 - \partial_y^2}\right) u \equiv F^{-1}\left\{\sqrt{\left(\frac{j\omega}{c}\right)^2 - (jk_y)^2}\,\tilde{u}(x, k_y, \omega)\right\} \tag{12.79}$$

Although sufficient for placing the pseudo-differential operator on some solid theoretical ground, Equation (12.79) is not directly usable in computations as the inverse Fourier transform is a global operation. Practical one-way wave equations are developed by seeking readily computable approximations to (12.79). To accomplish this, we take the approach followed in [18] and [19] and approximate the square root using a Taylor series expansion. First factor out a $(1/c)\partial_t$,

$$\left(\partial_x - \frac{1}{c}\partial_t\sqrt{1 - \frac{\partial_y^2}{\frac{1}{c^2}\partial_t^2}}\right) = 0 \tag{12.80}$$

We then note that waves incident on the boundary near normal incidence have $|k_x| \approx \omega/c >> |k_y|$. The operators are thus similarly related, $|\partial_x| \approx (1/c)\partial_t >> |\partial_y|$, and the square root can be approximated with a Taylor series. After multiplying through by the denominator, this results in

$$\left(\frac{1}{c}\partial_t\partial_x - \frac{1}{c^2}\partial_t^2 + \frac{1}{2}\partial_y^2\right) u = 0 \tag{12.81}$$

an approximate but computable one-way equation suitable for use on the left boundary.

Discretizing (12.71), the first-order or impedance condition for $-x$ propagating waves, results in the update equation

$$u_{0m}^{n+1} = u_{1m}^n - \frac{\Delta x - c\,\Delta t}{\Delta x + c\,\Delta t}(u_{1m}^{n+1} - u_{0m}^n) \tag{12.82}$$

where two-point difference approximations centered at $x = \Delta x/2, t = (n + 1/2)\,\Delta t$ have been used. Discretizing (12.81) and centering at $x = \Delta x/2, t = n\,\Delta t$ yield

$$\begin{aligned} u_{0m}^{n+1} = -u_{1m}^{n-1} - \frac{\Delta x - c\,\Delta t}{\Delta x + c\,\Delta t}(u_{0m}^{n-1} + u_{1m}^{n+1}) + \frac{2\,\Delta x}{\Delta x + c\,\Delta t}(u_{0m}^n + u_{1m}^n) \\ + \frac{\Delta x(c\,\Delta t)^2}{\Delta x + c\,\Delta t}\partial_y^2 u|_{(x,y)=(\Delta x/2, m\,\Delta y)}^{t=n\,\Delta t} \end{aligned} \tag{12.83}$$

Two marginally different discretizations of the second-order y derivative are used in [18] and [19]. Neither has a clear-cut accuracy or efficiency benefit. In Mur's implementation,

proper centering of this term is achieved by a spatial average in the x direction,

$$\partial_y^2 u|^{t=n\,\Delta t}_{(x,y)=(\Delta x/2,m\,\Delta y)} \approx \frac{1}{2}\left(\partial_y^2 u|^{t=n\,\Delta t}_{(x,y)=(0,m\,\Delta y)} + \partial_y^2 u|^{t=n\,\Delta t}_{(x,y)=(\Delta x,m\,\Delta y)}\right) \tag{12.84}$$

In contrast, Engquist and Majda average in both space and time:

$$\partial_y^2 u|^{t=n\,\Delta t}_{(x,y)=(\Delta x/2,m\,\Delta y)} \approx \frac{1}{2}\left(\partial_y^2 u|^{t=(n-1)\,\Delta t}_{(x,y)=(0,m\,\Delta y)} + \partial_y^2 u|^{t=(n+1)\,\Delta t}_{(x,y)=(\Delta x,m\,\Delta y)}\right) \tag{12.85}$$

In both cases, the second derivative is discretized using the standard three-point centered-difference approximation. Equation (12.83) is commonly referred to as a second-order Mur condition (or, more simply, Mur-2) by FDTD practitioners.

These discretized ABCs can be analyzed for their accuracy using a procedure similar to the dispersion analysis presented earlier. The finite-difference solution of two-dimensional second-order wave equations supports solutions of the form

$$u(t = n\,\Delta t, x = l\,\Delta x, y = m\,\Delta y) \equiv u_{lm}^n = e^{j\omega n\,\Delta t} e^{jk_x l\,\Delta x} e^{jk_y m\,\Delta y} \tag{12.86}$$

Return to the semi-infinite half-space FDTD grid, as shown in Figure 12.13, with an ABC imposed at $x = 0$. A steady-state, monochromatic plane wave with radian frequency ω impinges on the boundary at an angle θ measured from the $-x$ axis. Since any practical ABC is imperfect, a reflected wave is generated at $x = 0$. As the ABC must match the y variation of the incident field exactly and assuming no frequency conversion on reflection, the total solution is

$$u_{lm}^n = e^{j\omega n\,\Delta t}(e^{jk_x l\,\Delta x} + Re^{-jk_x l\,\Delta x})e^{-jk_y m\,\Delta y} \tag{12.87}$$

where k_x is assumed to be positive and the reflection coefficient R is to be determined. Equation (12.87) will then satisfy the discretized wave equation for all $l > 0$ for any value of R provided that the two-dimensional dispersion relation is satisfied. Note that the incidence angle θ is also related to the dispersion relation. For the positive-sign choice on k_x given above, $\theta = \tan^{-1}(k_y/k_x)$.

Substituting (12.87) into (12.83) gives a means of finding R,

$$R = -e^{jk_x\,\Delta x}\frac{\Delta x \sin(\omega\,\Delta t/2)\cos(k_x\,\Delta x/2) - c\,\Delta t\cos(\omega\,\Delta t/2)\sin(k_x\,\Delta x/2)}{\Delta x \sin(\omega\,\Delta t/2)\cos(k_x\,\Delta x/2) + c\,\Delta t\cos(\omega\,\Delta t/2)\sin(k_x\,\Delta x/2)} \tag{12.88}$$

where $\omega\,\Delta t$ and $k_x\,\Delta x$ are constrained by the dispersion relation (12.48). Applying the same procedure to the second-order Mur condition leads to

$$R = -e^{jk_x\,\Delta x} \times \frac{\Delta x[\sin^2(\omega\,\Delta t/2) - \frac{1}{2}(c\,\Delta t/\Delta y)^2\sin^2(k_y\,\Delta y/2)]\cos(k_x\,\Delta x/2) - c\,\Delta t\cos(\omega\,\Delta t/2)\sin(\omega\,\Delta t/2)\sin(k_x\,\Delta x/2)}{\Delta x[\sin^2(\omega\,\Delta t/2) - \frac{1}{2}(c\,\Delta t/\Delta y)^2\sin^2(k_y\,\Delta y/2)]\cos(k_x\,\Delta x/2) + c\,\Delta t\cos(\omega\,\Delta t/2)\sin(\omega\,\Delta t/2)\sin(k_x\,\Delta x/2)} \tag{12.89}$$

In Figure 12.14, reflection coefficients based on both the first- and second-order ABCs described above are shown for a typical case. The solid line is the first-order ABC (12.82) and the dashed line is the second-order ABC (12.83). Numerical parameters have been chosen to be similar to those commonly used in FDTD codes: $\Delta x = \Delta y$ (square cells), $c\,\Delta t = \Delta x/2$ (time step slightly smaller than the Courant stability limit), and $\omega/c = 2\pi/(10\,\Delta x)$ (cell width is one-tenth of a continuous free-space wavelength).

In the continuous case, both the first- and second-order ABCs are exact at normal incidence. In contrast, the discretized forms of these ABCs are, in general, not exact at normal incidence; $|R(\theta = 0)| \approx 0.02$ for the case shown in Figure 12.14. If the time

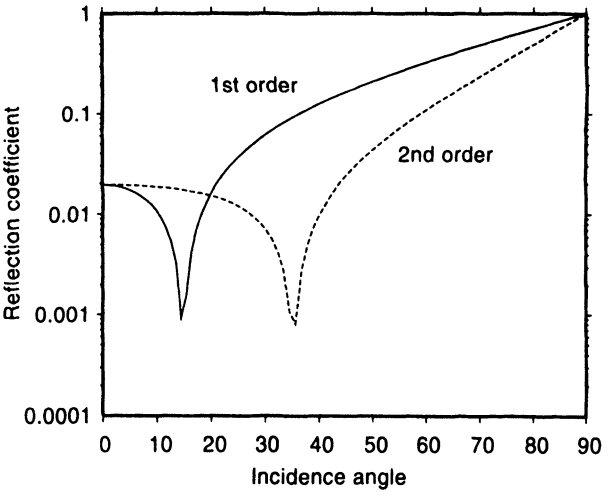

Figure 12.14 Magnitude of the reflection coefficient vs. incidence angle θ for two discretized ABCs. Solid line is the first-order Mur or impedance ABC and the dashed line is the second order Mur condition. Numerical parameters are $\Delta x = \Delta y, c\ \Delta t = \Delta x/2$, and $\omega/c = 2\pi/(10\ \Delta x)$.

step were chosen such that $c\ \Delta t = \Delta x$, the discretized ABCs would be exact at normal incidence. Unfortunately, this choice violates the stability criteria for the two-dimensional wave equation and thus cannot be used.

As the angle of incidence increases, the first-order ABC quickly fails while the second-order condition remains useful for a broader range of angles. Arbitrarily defining an ABC's useful range to be that range of angles where the magnitude of the reflection coefficient remains below 0.05, the first-order condition is seen to be useful up to $\theta = 28°$ and the second-order ABC can be used up to about 51°.

Figure 12.15 demonstrates the effect of the relative cell size on the ABC error. Here the reflection coefficient for the second-order Mur ABC [Equation (12.83)] is plotted as function of incidence angle for three different cell sizes: 5, 10, and 20 zones per continuous free-space wavelength. In each case, $\Delta x = \Delta y$ and $c\ \Delta t = \Delta x/2$. Large reflection coefficients are obtained on the coarse grid, even at near-normal incidence angles. As the grid resolution increases, the quality of the ABC increases and more nearly approximates the ideal case.

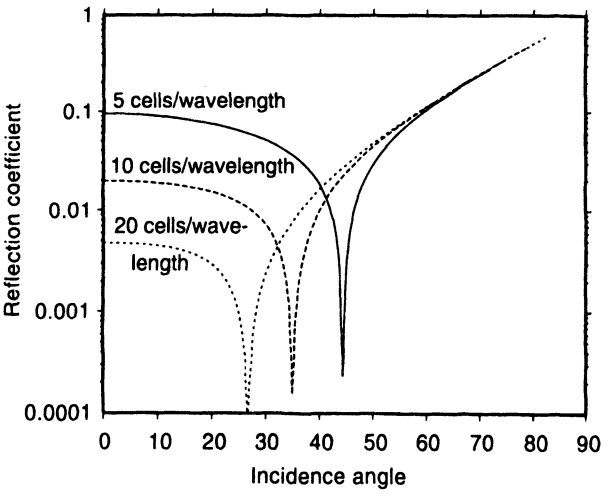

Figure 12.15 Magnitude of the reflection coefficient vs. incidence angle for the second-order Mur ABC with different grid resolutions. Numerical parameters are $\Delta x = \Delta y$ and $c\ \Delta t = \Delta x/2$.

Recent work by Bérenger [16] has revitalized interest in the use of absorbing materials as ABCs. Bérenger's particular approach, termed a perfectly matched layer (PML) in the literature, reduces unwanted reflections from the computational boundary to levels well below those offered by the Mur conditions. The PML is developed by first recognizing that a plane wave is perfectly matched (zero reflection) when normally incident on a half space with material properties

$$\frac{\sigma}{\epsilon_0} = \frac{\sigma^*}{\mu_0} \tag{12.90}$$

where σ^* is a magnetic conductivity. An open-region calculation can then be simulated in a finite-size FDTD grid by surrounding the region of interest with a layer of this lossy material; the layer serves as the absorbing material in a numerical anechoic chamber. The drawback of this approach is that the perfect match fails for waves that are not normally incident on the absorbing layer.

For the two-dimensional TE case, Bérenger overcame this drawback by artificially splitting the transverse magnetic fields into two subcomponents and associating independent magnetic conductivities with each subcomponent. Component-wise electrical conductivities are also introduced. The modified curl equations in the layer then become

$$\epsilon_0 \frac{\partial E_x}{\partial t} = \frac{\partial H_z}{\partial y} - \sigma_y E_x \tag{12.91}$$

$$\epsilon_0 \frac{\partial E_y}{\partial t} = -\frac{\partial H_z}{\partial x} - \sigma_x E_y \tag{12.92}$$

$$\mu_0 \frac{\partial H_{zx}}{\partial t} = -\frac{\partial E_y}{\partial x} - \sigma_x^* H_{zx} \tag{12.93}$$

$$\mu_0 \frac{\partial H_{zy}}{\partial t} = \frac{\partial E_x}{\partial y} - \sigma_y^* H_{zy} \tag{12.94}$$

where $H_z = H_{zx} + H_{zy}$ and σ_x^* and σ_y^* are the component-wise magnetic conductivities. The impact of this particular field/conductivity splitting is that the perfect match is maintained at the free space–PML boundary regardless of incidence angle. For example, in truncating an FDTD grid on the right (outgoing normal direction $= \hat{x}$) boundary, set $\sigma_y = \sigma_y^* = 0$ and let $\sigma_x = \sigma_x^* \epsilon_0 / \mu_0$ be a constant. Time-harmonic $+x$-directed solutions in the PML region are

$$H_z = H_0 e^{j\omega t} e^{-j(\omega/c)(x\cos\phi + y\sin\phi)} e^{-(\sigma_x \cos\phi/\epsilon_0 c)x} \tag{12.95}$$

$$\mathbf{E} = (-\hat{x}\sin\phi + \hat{y}\cos\phi)\sqrt{\frac{\mu_0}{\epsilon_0}} H_z \tag{12.96}$$

The form of this solution permits reflectionless transmission into the PML. Energy is dissipated through the exponential decay factor.

When the conductivities in the PML are large, fields decay rapidly and the linear differencing used in the core FDTD algorithm is no longer appropriate. Instead exponential differencing is used. The update equation corresponding to (12.92) is

$$E_y^{n+1}(i, j+\tfrac{1}{2}) = e^{-\sigma_x \Delta t/\epsilon_0} E_y^n(i, j+\tfrac{1}{2}) - \frac{1}{\sigma_x}(1 - e^{-\sigma_x \Delta t/\epsilon_0}) \frac{H_z^{n+1/2}(i+\frac{1}{2}, j+\frac{1}{2}) - H_z^{n+1/2}(i-\frac{1}{2}, j+\frac{1}{2})}{\Delta x} \tag{12.97}$$

An infinitely thick absorbing layer is, of course, impractical in a real FDTD application. The simplest solution is to terminate the PML after some distance sufficient to absorb most of the outgoing energy with a simple boundary condition such as a p.e.c. This has the impact of returning a small portion of the outgoing electromagnetic energy into the computational space, thus introducing some error. A second practical issue concerns the thickness of the PML itself. As these cells are added on the exterior of the FDTD region of interest, their number grows rapidly as the thickness increases, especially in three-dimensional applications. Considerable research effort has thus been spent in determining material profiles in the PML that minimize its thickness while maintaining its accuracy. Readers are referred to [22] for details.

12.13 INTERNAL AND EXTERNAL SOURCES

Having developed the core algorithm and a way of getting the waves out of the FDTD box, we next examine methods for driving the FDTD problem space via incident fields and internal sources. One simple source model to include is that of a driven current. Let the current density $\mathbf{J}(\bar{r}, t)$ be specified. Then, maintaining consistency in the time discretization,

$$\epsilon_0 \dot{\mathbf{E}}^{n-1/2} = \nabla \times \mathbf{H}^{n-1/2} - \mathbf{J}^{n-1/2} \tag{12.98}$$

where the standard spatial discretization is used. Note that the current source is located at the same spatial point as the electric field but at the same time point as the magnetic field. Another simple source is a driven voltage gap, such as might occur at an antenna feed. Assume a voltage source applied over a one-cell wide gap in the y direction. Then,

$$E_y^n(i, j) = \frac{V(t = n\,\Delta t)}{\Delta y} \tag{12.99}$$

These methods can be extended to include lumped circuit elements along with the driven sources [8].

A source of external plane waves is required for scattering and coupling applications. As mentioned briefly in Section 12.11, the FDTD can be formulated in terms of either total or scattered fields. While there are advantages to either approach, we have focused on the total-field formulation in this chapter, largely because the handling of p.e.c. boundaries and penetrable materials is straightforward. The use of an ABC, which is designed to remove waves from the FDTD problem space, would appear to be in conflict with the excitation of the incident field in a total-field code. The solution is to divide the problem space as shown in Figure 12.16 into an internal total-field region containing the scattering/coupling object and an external layer of cells containing the scattered field. Since the scattered-field region contains outgoing waves only, an ABC can successfully be placed on the external boundary. To apply the plane-wave source, let the fields on the total–scattered field interface be total fields, as shown in Figure 12.17. The curl equations used to update these fields must then also use total fields. Since only scattered fields are stored in the exterior domain, the FDTD update equations must be modified to add in the incident field to these components. A similar modification is also made to the update equations for the scattered-field components immediately outside the interface. Although the incident field can be calculated analytically, a better solution is obtained by calculating the incident field on a separate (usually one-dimensional) FDTD grid that approximately matches the dispersion characteristics of the main grid.

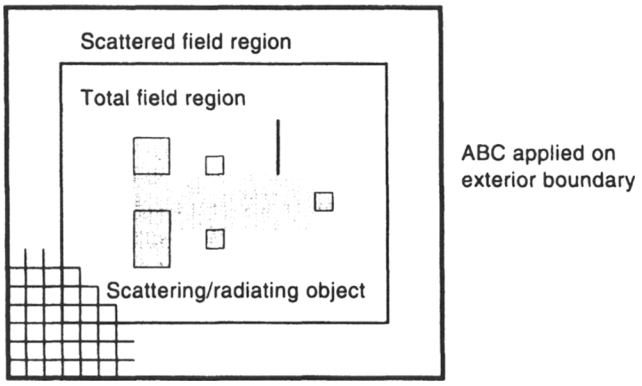

Figure 12.16 Division of the FDTD problem space into an interior total-field region that contains the interacting object(s) and an exterior scattered-field region that permits straightforward implementation of the ABC.

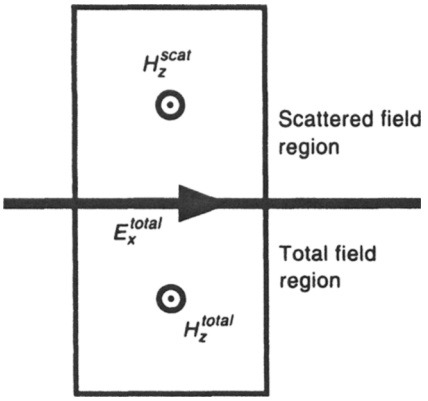

Figure 12.17 Field variables on and adjacent to the total field–scattered field interface.

12.14 FAR-FIELD PROJECTIONS

The FDTD method as developed so far in this chapter suffices for simulating the fields within the computational volume. However, for radiation and scattering calculations we must develop a method for calculating far fields, well outside the computational domain. The approach is conceptually straightforward. Referring to Figure 12.18, define a computational surface inside the FDTD grid that encloses the scattering or radiating object. For simplicity in the subsequent far-field projection equations and in programming the method, this volume is usually rectangular. Tangential electric and magnetic fields are captured on this surface and converted to equivalent surface currents via

$$\mathbf{J}_s = \hat{n} \times \mathbf{H} \tag{12.100}$$

$$\mathbf{M}_s = \mathbf{E} \times \hat{n} \tag{12.101}$$

where $\hat{n}$ is the surface unit outward normal. Fields at any arbitrary point outside this surface can then be computed using vector potentials [23] or the Stratton–Chu representation theorem [24] or by treating the equivalent currents as an array of Hertzian dipoles [25]. The

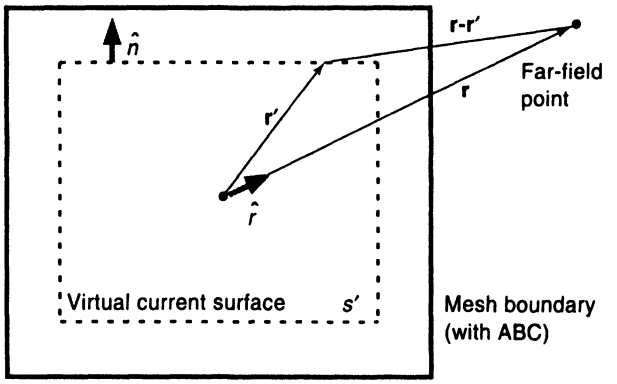

Figure 12.18 Geometry for FDTD far-field projection.

standard far-field approximations are employed to simplify the calculations.

The simplest form of the far-field projection equations occurs in the "time-harmonic" style of FDTD simulations proposed by Taflove [4]. In this method, the excitation is driven with a sine wave at the appropriate frequency and the FDTD simulation is run to steady state. Magnitude and phase information on the equivalent current surface is determined by sampling the last cycle of the sine wave at each measurement point. The frequency-domain form of the vector potentials can then be used to compute far fields.

Other authors use broadband excitations, either because they are interested in the time-varying nature of the solution itself or because broadband frequency-domain results can readily be obtained through a Fourier transform. Time-domain far-field projection algorithms are, however, somewhat more complicated than their frequency-domain counterparts; the equations contain a temporal derivative of the equivalent surface currents. In addition, a proper accounting must be made of the angle-dependent time delays involved in integrating over a spatially distributed source.

To examine these issues, refer to Figure 12.18 for geometry and notation. In the far field, the transverse electric field can be written in terms of the vector potentials as

$$E_\theta = -\mu \frac{\partial A_\theta}{\partial t} - \frac{1}{c}\frac{\partial F_\phi}{\partial t} \tag{12.102}$$

$$E_\phi = -\mu \frac{\partial A_\phi}{\partial t} + \frac{1}{c}\frac{\partial F_\theta}{\partial t} \tag{12.103}$$

where the θ and ϕ subscripts denote vector components in three-dimensional spherical coordinates. Under the standard the far-field approximations, the vector potentials take on the form

$$\mathbf{A} = \frac{1}{4\pi r}\int_{s'} \mathbf{J}_s\left[\mathbf{r}', t - (r - \hat{r}\cdot\mathbf{r}')/c\right] ds' \tag{12.104}$$

$$\mathbf{F} = \frac{1}{4\pi r}\int_{s'} \mathbf{M}_s\left[\mathbf{r}', t - (r - \hat{r}\cdot\mathbf{r}')/c\right] ds' \tag{12.105}$$

where s' denotes the equivalent current surface and the $(r - \hat{r}\cdot\mathbf{r}')/c$ term accounts for the propagation time difference between the origin and the integration point. Note that the use of the equivalence principle requires that $\mathbf{J}_s$ and $\mathbf{M}_s$ be defined on the same surface. Simple averaging is thus used to colocate the spatially staggered FDTD fields.

The far-field projection problem then reduces to one of developing efficient methods for computing (12.104) and (12.105) and/or their temporal derivatives. The key complicating feature is the presence of the integration point $\mathbf{r}'$ in the time delay. The result is that the instantaneous far-field values need to be computed via accumulation over a series of time steps. The length of the accumulation period corresponds to the projected length of the equivalent current source.

A practical challenge is encountered when determining whether to perform the far-field calculations during the FDTD simulation or to save the equivalent currents for subsequent postprocessing. Storing the currents provides the most flexibility but incurs significant storage costs. If the number of desired far-field projection angles and/or frequencies is reasonable, then it generally makes sense to perform the calculations on the fly. Kunz and Luebbers [8] provide a good discussion of the trade-offs between these factors.

12.15 EXTENSIONS TO THE ORTHOGONAL MESH FDTD METHOD

The FDTD method has been used successfully to solve a large number of electromagnetic problems. However, the technique has certain limitations, stemming largely from the use of the uniform orthogonal mesh. This restriction forces curved and diagonal boundaries to be represented by staircased approximations. Various groups have developed FDTD-like algorithms that can be used on nonorthogonal boundary conforming meshes. Approaches include curvilinear coordinate variants of the FDTD [26–28], finite-volume methods [29], and a discrete-surface integral method [30]. These methods allow greater geometric flexibility but incur a higher computational cost. Subgridding approaches have also been explored [31, 32]. These methods allow the orthogonal mesh to be retained throughout most of the computational domain but permit local refinement where needed.

Another successful area of research has been in the development of subcell methods [8, Chapter 10; 33, 34]. These methods modify the difference equations locally, adding algorithms that permit accurate modeling of structures such as wires or slots that are, in at least one dimension, too small to be handled efficiently by the unmodified FDTD method.

REFERENCES

[1] C. L. Bennett and W. L. Weeks, "Transient scattering from conducting cylinders," *IEEE Trans. Antennas Propagat.*, vol. AP-18, pp. 627–633, Sept. 1970.

[2] S. M. Rao and D. R. Wilton, "Transient scattering by conducting surfaces of arbitrary shape," *IEEE Trans. Antennas Propagat.*, vol. AP-39, pp. 56–61, Jan. 1991.

[3] K. S. Yee, "Numerical solution of initial boundary value problems involving Maxwell's equations in isotropic media," *IEEE Trans. Antennas Propagat.*, vol. AP-14, pp. 302–307, May 1966.

[4] A. Taflove and M. E. Brodwin, "Numerical solution of steady-state electromagnetic scattering problems using the time-dependent Maxwell's equations," *IEEE Trans. Microwave Theory Tech.*, vol. MTT-23, pp. 623–630, Aug. 1975.

[5] R. Holland, "Threde: A free-field EMP coupling and scattering code," *IEEE Trans. Nucl. Sci.*, vol. NS-24, pp. 2416–2421, Dec. 1977.

[6] K. Kunz and K. M. Lee, "A three-dimensional finite-difference solution of the external response of an aircraft to a complex transient EM environment: Part I—the method and its implementation," *IEEE Trans. Electromagnet. Compat.*, vol. EMC-20, pp. 328–333, May 1978.

[7] D. E. Merewether and R. Fisher, "Finite difference solution of Maxwell's equation for EMP applications," Electro Magnetic Applications Inc. report EMA-79-R-4, Defense Nuclear Agency, 1980.

[8] K. S. Kunz and R. J. Luebbers, *The Finite Difference Time Domain Method for Electromagnetics*, CRC Press, Boca Raton, FL, 1993.

[9] A. Taflove, *Computational Electrodynamics: The Finite-Difference Time-Domain Method*, Artech House, Norwood, MA, 1995.

[10] A. Taflove and K. R. Umashankar, "The finite-difference time-domain method for numerical modeling of electromagnetic wave interactions with arbitrary structures," in *Pier 2: Progress in Electromagnetics Research*, Elsevier, New York, 1990.

[11] K. L. Shlager and J. B. Schneider, "A selective survey of the finite-difference time-domain literature," *IEEE Antennas Propagat. Mag.*, vol. 37, pp. 39–57, Aug. 1995.

[12] J. Fang, "Time domain finite difference computation for Maxwell's equations," Ph.D. dissertation, University of California at Berkeley, 1989.

[13] R. Luebbers, F. Hunsberger, K. Kunz, R. Standler, and M. Schneider, "A frequency-dependent finite-difference time-domain formulation for dispersive media," *IEEE Trans. Electromagnet. Compat.*, vol. EMC-32, pp. 222–227, Mar. 1990.

[14] R. M. Joseph, S. C. Hagness, and A. Taflove, "Direct time integration of Maxwell's equations in linear dispersive media with absorption for scattering and propagation of femtosecond electromagnetic pulses," *Opt. Lett.*, vol. 16, pp. 1412–1414, Sept. 1991.

[15] R. F. Harrington, *Time-Harmonic Electromagnetic Fields*, McGraw-Hill, New York, 1961.

[16] J. P. Bérenger, "A perfectly matched layer for the absorption of electromagnetics waves," *J. Computat. Phys.*, vol. 114, pp. 185–200, Oct. 1994.

[17] E. L. Lindman, "'Free space' boundary conditions for the time dependent wave equation," *J. Computat. Phys.*, vol. 18, pp. 67–78, 1975.

[18] B. Engquist and A. Majda, "Absorbing boundary conditions for the numerical simulation of waves," *Math. Comp.*, vol. 31, pp. 629–651, July 1977.

[19] G. Mur, "Absorbing boundary conditions for the finite-difference approximation of the time-domain electromagnetic field equations," *IEEE Trans. Electromagnet. Compat.*, vol. EMC-23, pp. 377–382, Nov. 1981.

[20] R. L. Higdon, "Absorbing boundary conditions for difference approximations to the multi-dimensional wave equations," *Math. Computat.*, vol. 47, pp. 437–459, 1986.

[21] Z. P. Liao, H. L. Wong, B.-P. Yang, and Y.-F. Yuan, "A transmitting boundary for transient wave analysis," *Sci. Sinica, Ser. A*, vol. 27, pp. 1063–1076, 1984.

[22] J. P. Bérenger, "Improved PML for the FDTD solution of wave-structure interaction problems," *IEEE Trans. Antennas Propagat.*, vol. 45, pp. 466–473, Mar. 1997.

[23] R. J. Luebbers, K. S. Kunz, M. Schneider, and F. Hunsberger, "A finite-difference time-domain near zone to far zone transformation," *IEEE Trans. Antennas Propagat.*, vol. 39, pp. 429–433, Apr. 1991.

[24] K. S. Yee, D. Ingham, and K. Shlager, "Time-domain extrapolation of the far field based on FDTD calculations," *IEEE Trans. Antennas Propagat.*, vol. 39, pp. 410–413, Mar. 1991.

[25] M. J. Barth, R. R. McLeod, and R. W. Ziolkowski, "A near and far-field projection algorithm for finite-difference time-domain codes," *J. Electromagnet. Waves Applicat.*, vol. 6, pp. 5–18, 1992.

[26] R. Holland, "Finite difference solutions of Maxwell's equations in generalized nonorthogonal coordinates," *IEEE Trans. Nucl. Sci.*, vol. NS-30, pp. 4589–4591, Dec. 1983.

[27] M. Jones, "Electromagnetic PIC codes with body-fitted coordinates," *Proceedings of the 12th Conference on the Numerical Simulation of Plasmas*, American Physical Society, Topical Group on Computational Physics, San Francisco, CA, Sept. 20–23, 1987.

[28] M. Fusco, "FDTD algorithm in curvilinear coordinates," *IEEE Trans. Antennas Propagat.*, vol. AP-38, pp. 76–89, Jan. 1990.

[29] N. Madsen and R. W. Ziolkowski, "A three-dimensional modified finite volume technique for Maxwell's equations," *Electromagnetics*, vol. 10, pp. 147–161, 1990.

[30] N. Madsen, "Divergence preserving discrete surface integral methods for Maxwell's curl equations using non-orthogonal unstructured grids," *J. Computat. Phys.*, vol. 119, pp. 34–45, 1995.

[31] K. S. Kunz and L. Simpson, "A technique for increasing the resolution of finite-difference solutions of the Maxwell equations," *IEEE Trans. Electromagnet. Compat.*, vol. EMC-23, pp. 419–422, Apr. 1981.

[32] S. S. Zivanovic, K. S. Yee, and K. K. Mei, "A subgridding algorithm for the time-domain finite-difference method to solve Maxwell's equations," *IEEE Trans. Microwave Theory Tech.*, vol. MTT-38, pp. 471–479, Mar. 1991.

[33] K. R. Umashankar, A. Taflove, and B. Beker, "Calculation and experimental validation of induced currents on coupled wires in an arbitrarily shaped cavity," *IEEE Trans. Antennas Propagat.*, vol. AP-35, pp. 1248–1257, Nov. 1987.

[34] D. J. Riley and C. D. Turner, "Hybrid thin-slot algorithm for the analysis on narrow apertures in finite-difference time-domain calculations," *IEEE Trans. Antennas Propagat.*, vol. AP-38, pp. 1943–1950, Dec. 1990.

PROBLEMS

P12.1 Discretize the one-dimensional second-order, single field, wave equation (see Equation 12.9) using three-point centered difference approximations to the spatial and temporal second-order derivatives. Show that this discretization is equivalent to the one-dimensional FDTD equations.

P12.2 Assuming staggered field locations as used in the FDTD method, use rooftop basis functions and razor blade test functions to derive the FDTD spatial discretization. Outline how this approach might be used to extend the FDTD method to nonorthogonal meshes.

P12.3 Use the integral form of Maxwell's equations to derive an FDTD-discretization on a uniform mesh of equilaterial triangles.

P12.4 Develop the FDTD equations for the two-dimensional TM case.

P12.5 Derive the one-dimensional dispersion relation and stability conditions for the FDTD equations in conductive media. Derive an approximate dispersion relation in the low-loss case ($\sigma \Delta t / 2\varepsilon << 1$). Some authors use a non-centered approximation to the

conductive loss term in Equation (12.49), replacing $\sigma \mathbf{E}^{n-1/2}$ with $\sigma \mathbf{E}^{n-1}$. What impact does this have on dispersion and stability?

P12.6 Show that the time-harmonic PML solutions (12.95)–(12.96) satisfy the PML partial differential Equations [(12.91)–(12.94), with $\sigma_y = \sigma_y^* = 0$ and $\sigma_x = \sigma_x^* \varepsilon_0 / \mu_0$]. Consider a time-harmonic plane wave traveling in free space and obliquely incident on a PML half space. Derive the reflection and transmission coefficients as a function of incidence angle; ignore spatial and temporal discretization.